Effect of Defect Density Variation in CdTe Solar Cell Using Cu as A Hole Transport Layer and Back Contact

F. T. Johora[1], M. A. Khan[1*], A. Al Asad[1], Md. Rabiul Islam[1] and A. Rayhan[1]
[1]Dept. of Electrical and Electronic Engineering, BSMRSTU, Gopalganj-8100, Bangladesh.
*Corresponding author's email: asad.khan@bsmrstu.edu.bd, arzu1013@gmail.com

Abstract – *Cadmium Telluride (CdTe) solar cells have the potential to achieve high efficiency, but material defects present a significant challenge to their performance. These defects act as recombination sites, capturing electrons and holes, thereby hindering current flow and reducing the overall efficiency of the CdTe solar cells. Addressing these defects is crucial for enhancing charge carrier transport and optimizing efficiency. This research paper analyzes the effect of defect density numerically using SCAPS-1D simulation software on SnO_2/CdTe/CdS/Cu multi-junction structural solar cells. The performance parameters of the proposed cell are optimized by varying different numerical particulars. Our analysis reveals that by varying the defect density from 10^{12} to 10^{18} cm^{-3}, the efficiency of the proposed solar cells varies from 17.65% to 2.56%, with the open-circuit voltage (Voc) at 0.85V, short-circuit current density (Jsc) at 26 mA/cm², and fill factor (FF) at 82%. The efficiency optimization is attributed to the conduction band effective density of states, Nc = 2.2 × 10^{18} cm^{-3}, and valence band effective density of states, Nv = 1.8 × 10^{19} cm^{-3} of the donor material (SnO_2). The cell's power conversion efficiency is optimized when the absorber has a balanced concentration of neutral, acceptor, and donor defects at 1 × 10^{14} cm^{-3}. At an operating temperature of 300 K, an efficiency of 18% is achieved.*

Keywords: *Cadmium telluride (CdTe) solar cell, Defect density, Recombination sites, Solar cell performance*

Article History
Received 1 June 2024
Received in revised form 3 July 2024
Accepted 9 September 2024

I. Introduction

Research on CdTe solar cells has been ongoing since the mid-20th century to improve their efficiency for enhanced solar energy utilization [1]. These cells are of great interest due to their excellent performance. Recent studies have shown that their efficiency can exceed 22% [2] – [4]. CdTe solar cells are considered to be one of the most promising solar cell technologies for the future. They are relatively inexpensive to manufacture due to abundant raw materials, simple manufacturing processes, thin-film technology requiring less material, and scalable production and have a high absorption coefficient of 5 × 10^5 cm^{-1}, which means that they can absorb a large amount of sunlight approximately 400 to 800 nanometers (nm). The direct band gap of CdTe (1.5 eV) is also well-matched to the solar spectrum, which means that it can absorb photons from a wide range of wavelengths. This makes CdTe solar cells a very efficient way to convert sunlight into electricity [5] – [6]. Incorporating desirable attributes of CdTe's absorption characteristics, the presence of n-type material is imperative for the optimal formation of a high-quality p-n junction. Notably, Cadmium Sulphide (CdS) stands out as a prominent candidate, showcasing exceptional capabilities due to its direct band-gap of approximately 2.42 eV within the visible spectrum.

The transparent nature of CdS enables solar irradiation to transmit through the CdTe layer, thereby enhancing the photovoltaic response. [7] – [8]. Conversely, the heterojunction CdTe/CdS solar cell necessitates the integration of a transparent conducting oxide (TCO) layer at its front contact. This strategic inclusion allows photons to enter the cell, with the active interface acting as an electrode to efficiently collect the generated current. [9] – [11]. Notably, transparent conducting oxide (TCO) layers commonly employed for this purpose include Fluorine-doped Tin Oxide (SnO_2:F or FTO) and Aluminum-doped Zinc Oxide (ZnO: Al or AZO) [12] – [13]. These materials play a pivotal role in enabling photon transmission and effectively harnessing current at the active interface of the heterojunction CdTe/CdS solar cell [14] – [15]. Incorporating a high-resistive transparent (HRT) film

between the transparent conducting oxide (TCO) and the CdS buffer layer holds the potential to enhance efficiency by mitigating the impact of non-uniformity [16]. This approach effectively minimizes variations that may arise, contributing to a more consistent and optimized performance of the solar cell [17]. Undoped Tin Oxide (i-SnO_2) and undoped Zinc Oxide (i-ZnO) stand out as materials frequently employed for the development of a high-resistive transparent (HRT) layer [18, 19]. This layer serves a crucial role in enhancing the solar cell's performance by reducing the impact of non-uniformity, thereby contributing to a more consistent and efficient operation [20] – [21].

During the 1980s, T. P. Shalvey et. al. and others focused on the back surface field (BSF) layer and its consequential influence on the efficiency of solar cells [22] – [24]. These studies delved into the effects and potential benefits of implementing a BSF layer in photovoltaic devices, aiming to optimize energy conversion and enhance overall solar cell performance [25] – [26]. A material with a substantial band gap is strategically used as a barrier at the CdTe/BSF heterojunction [27] – [28]. This barrier effectively prevents carriers from dissipating at the back contact interface [29]. By minimizing carrier losses, this approach enhances the overall efficiency of the photovoltaic system [30].

Furthermore, this approach mitigates carrier recombination at the back contact interface, resulting in an enhancement of cell efficiency [31] – [32]. By curbing the tendency for carriers to recombine at this junction, the overall performance of the solar cell is notably improved [33] – [34]. Within the same scholarly framework, investigations have established that the utilization of a hole transport-electron blocking layer (HT-EBL) parallels the role fulfilled by the back surface field (BSF) layer [35] – [36]. This layer, the HT-EBL, effectively reduces carrier losses and mitigates recombination phenomena at the rear contact interface [37]. As a result, the discernible consequence manifests as an enhancement in the efficiency of solar cells. Additionally, it substantiates a significant contribution toward the elevation of the solar cell's operational efficacy. A notably promising candidate material employed as a hole transport-electron blocking layer (HT-EBL) within CdTe solar cells is cuprous oxide (Cu_2O) [38, 39]. A notably promising material used as a hole transport-electron blocking layer (HT-EBL) in CdTe solar cells is cuprous oxide (Cu_2O) [37] – [38]. With a wide band gap ranging from 2.1eV to 2.61 eV and natural p-type conductivity, cuprous oxide has characteristics that make it suitable for this purpose [39] – [40].

Cu_2O is non-toxic, making it environmentally friendly. It is also readily available, cost-effective, and has a high absorption coefficient in the visible spectrum, making it a good choice for solar cells [40]. However, defects in CdTe solar cells can limit their efficiency. Common defects include grain boundaries, impurities, and dislocations, which can create recombination centers for charge carriers, reducing the overall performance of the cell [41].

In the proposed SnO_2/CdS/CdTe/Cu model, copper (Cu) serves a dual purpose as both the back contact and an electrode, thereby facilitating the accumulation and directed flow of generated electrons from the CdTe layer into the external circuit. This orchestrated movement of electrons forms the fundamental basis for the overarching process of electricity generation. It is pertinent to underscore that the inclusion of copper at the back contact interface exerts a notable influence on carrier recombination phenomena. Acting as an effective electron-blocking layer, the Cu layer prevents photo-generated electrons from recombining at the rear surface. This process increases the retention of generated charge carriers, thereby improving the efficiency of energy conversion.

In summary, the strategic addition of copper in the SnO_2/CdS/CdTe/Cu model has two main effects: it enhances charge collection and reduces carrier recombination. This combination leads to an overall increase in the efficiency of the photovoltaic device.

II. Solar Cell Structure and Materials Properties

Fig.1 depicts the schematic configuration of a SnO_2/CdS/CdTe/Cu heterojunction solar cell. The cell primarily consists of a CdS(n)/CdTe(p) heterojunction, with n-type and p-type doping concentrations of 1×10^{18} cm^{-3} and 2×10^{14} cm^{-3}, respectively, forming the core structure. An optically transparent SnO_2 film functions as the high-resistive transparent (HRT) layer situated between the transparent conducting oxide (TCO) and CdS regions. The back contact is established through a copper (Cu) layer. Key constituents include CdS and CdTe layers, serving as the window and absorber materials, respectively. Cu and FTO materials fulfill distinct roles as the rear contact (anode) and the front contact (cathode), respectively. The FTO layer on the glass substrate is characterized by a thickness of 1 mm, a refractive index of 1.52, and a front surface reflection coefficient of 4.22%. In this context, parameters such as thickness, carrier concentration, interface defect density, and operational temperature have been meticulously chosen as focal considerations.

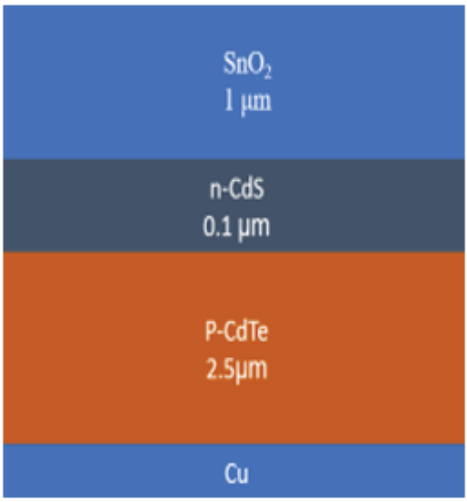

Fig. 1. FTO/CdS/CdTe/Cu solar cell model

To facilitate simulation, the glass/TCO substrate is modeled as an FTO layer, specified with a thickness of 300 nm [42] and an n-type doping concentration of 3×10^{20} cm^{-3}. Comprehensive device geometrical and physical attributes are shown in Table I for reference and analysis. The absorber layer in solar cells is made up of CdTe, which has a high absorption coefficient of over 10^4 cm^{-1} and an ideal direct band gap of 1.45 eV for effective photo conversion at room temperature [43] – [44]. To form a p-n junction, p-type CdTe is often paired with n-type CdS, which serves as the window layer in the heterojunction [45] – [46]. The absorber layer may contain acceptor defects because of its p-type characteristics, which can lead to a reduction in solar cell efficiency. CdS serves as the window layer and is commonly used in CdTe photovoltaic devices [46]. This layer facilitates Cadet Nucleation and growth and creates a high-quality heterojunction with the absorber shown this band alignment from the energy band diagram on SCAPS [47]. At room temperature, CdS has a direct bandgap of 2.42 eV and exhibits an acceptable lattice mismatch of 9.7% with CdTe [48]. This layer is n-type so donor defects are found in this layer. The band gap of CdS, measuring 2.42 eV, signifies its capability to facilitate relatively unimpeded transmission of a significant portion of the solar spectrum. This attribute renders it an apt choice as a window layer situated atop the absorber. Herein, the occurrence of photo-generated surplus minority carriers finds an advantageous environment for its manifestation, a concept underscored by Coutts (1982). In the context of CdTe, it manifests as a direct band gap semiconductor at 1.5 eV. To construct solar cells based on CdTe, films of this material measuring 2.5 µm in thickness are employed [47].

TABLE I
DEVICE PARAMETERS USED IN THE SIMULATION

Parameters	**Layers**			
	CdTe	**CdS**	**SnO_2**	**FTO** [17]
Thickness, t_m(nm)	2500 [47]	100	1000	300
Electron affinity, χ_e (eV)	3.9	10	4	3.2
Dielectric ratio, ε_r	9.4	4	9	4.4
Band gap, E_g (eV)	1.45	2.42	3.63	9
Conduction band effective density of states, N_c (cm^{-3}) [17]	8×10^{17}	2.2×10^{18}	2.2×10^{18}	2.2×10^{18}
Valance band effective density of states, N_v (cm^{-3})	1.8×10^{19}	1.8×10^{19}	1.8×10^{19}	1.8×10^{19}
Electron mobility, μ_n (cm^2/Vs)	320	100	100	90
Hole mobility, μ_p (cm^2/Vs)	40	25	25	90
Carrier concentration, N_a (cm^{-3})	2×10^{14}	0	0	3×10^{20}
Carrier concentration, N_d (cm^{-3})	0	1.1×10^{18}	1×10^{17}	0
Hole lifetime (ns)	1	0.01	0.1	1×10^{15}
Electron lifetime (ns)	1	0.01	100	

The collective assortment of parameters crucial for the design of the SnO_2/CdS/CdTe/Cu configuration is comprehensively shown in Table I. This authors have chosen a 0.25 cm^2 area for this device. The simulation was conducted with an incident irradiation of 1000 W/m^2.

The investigation at hand employs SCAPS-1D for modeling and numerical simulation of the

SnO_2/CdS/CdTe/Cu heterojunction solar cell. SCAPS-1D effectively facilitates the analysis of the J–V (current-voltage) characteristics and quantum efficiency of the solar cell. This software affords a comprehensive platform for discerning and quantifying the performance aspects of the studied system. The utilization of SCAPS-1D involves a meticulous exploration and comparison of defects within CdTe solar cells, featuring similar parameters albeit distinct layers (CdTe & CdS). Given the crystalline nature of CdS and CdTe, their physical attributes exhibit variability contingent upon growth conditions and fabrication techniques employed. Within the scope of this study, it is pivotal to underscore that the parameters of the absorber and window layers remain constant, aligning precisely with the values outlined in Table I. This consistency is upheld throughout all simulation steps, ensuring robustness and accuracy. The parameters requisite for all four materials under examination have been diligently furnished. Meanwhile, a copper layer boasting a work function of 5 eV serves as the back contact, an operating temperature of 300K, and a total number of simulations have been carried out with a series resistor of 3.2 Ω and a shunt resistor of 3200 Ω.

III. Results and Discussion

We conducted an analysis focusing on two distinct types of defects: acceptor and donor—present within the CdTe and CdS layers. Our assessment encompassed the calculation of various critical parameters, encompassing efficiency, open-circuit voltage (Voc), short-circuit current density (Jsc), and fill factor (FF), employing the SCAPS platform. The range of defect densities scrutinized extended from 10^{12} to 10^{18}. It emerges that acceptor defects are predominant within the CdTe layer, whereas donor defects are primarily concentrated within the CdS layer. Notably, defect densities beneath 10^{12} cm^{-3}, exhibited minimal impact on the percentage of the power conversion efficiency (PCE) for both layers. However, a discernible reduction in all parameters was observed as defect density exceeded the 10^{12} cm^{-3}, threshold. This decrement was found to be more pronounced in the CdTe layer compared to the CdS layer. At a defect density of 10^{18} cm^{-3}, the lowest values for Voc, Jsc, FF, and PCE were identified. These outcomes collectively underscore the correlation between heightened defect density and diminished solar cell performance. The findings validate the notion that the augmentation of defect density invariably precipitates a decline in the operational efficiency of the solar cell.

A. Effect of the Acceptor Defect Density within the CdTe Absorber Layer

Our simulation outcomes indicate that Acceptor defects have a greater impact on cell performance. In Fig. 2. it is clear that acceptor defects elicit a profound transformation across all parameters. Efficiency precipitously declines from 17.65% to 2.56%, and the fill factor undergoes a substantial reduction, descending from 84.77% to 49.87%. This discernible divergence is rooted in the energy band diagram for the CdTe solar cell incorporating defects. Our analysis vividly elucidates that the introduction of defects engenders trap levels. The nature of these trap levels evolves, transitioning from lying beneath the Fermi level of electrons for lower defect densities to situating between the Fermi level of electrons and the conduction band energy level at a defect density of 10^{18} cm^{-3}. Consequently, the phenomenon of photo-generated electrons becoming ensnared at these energy levels ensues, thereby manifesting as a diminishment in the photovoltaic efficacy of CdTe solar cell devices.

Another explanatory facet resides in the absorber layer's role. The augmentation of efficiency correlates closely with the characteristics of the absorber layer. Consequently, the influence of increased defect density is more pronounced within the absorber layer, further substantiating the observed dissimilarity in the impact of acceptor and donor defects.

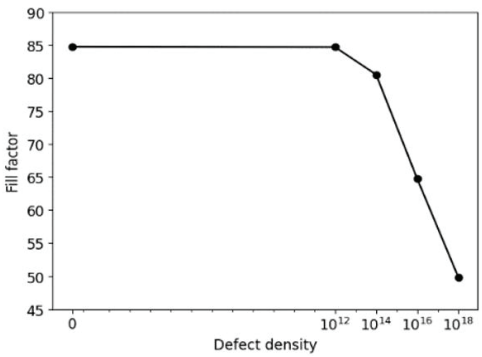

(a) Variation of Fill factor (FF) vs Defect density

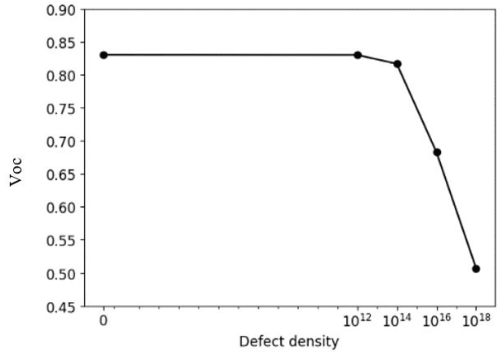

(b) Variation of open-circuit voltage (Voc) vs Defect density

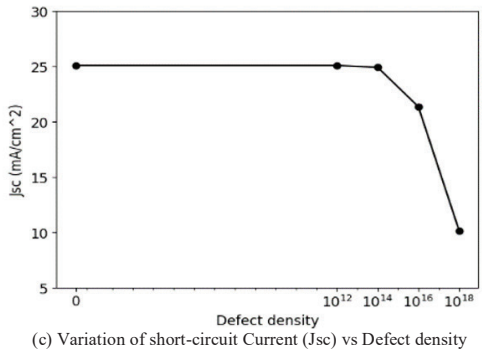

(c) Variation of short-circuit Current (Jsc) vs Defect density

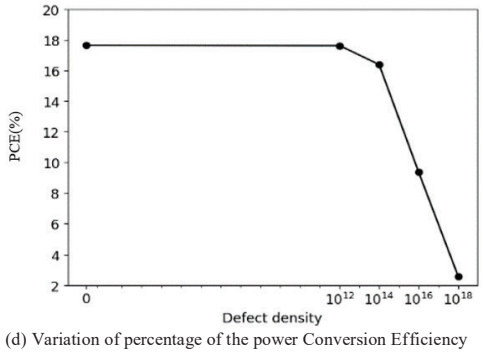

(d) Variation of percentage of the power Conversion Efficiency (PCE%) vs Defect density

Fig. 2. Effect of the acceptor defect density on FF, Jsc, Voc, and PCE(%) in the CdTe absorber layer.

B. Effect of the Donor Defect Density in CdS Window Layer

In our observations, a notable trend emerges regarding the impact of defect density on efficiency within the CdTe absorber layer. The efficiency demonstrates a marked reduction, declining from 17.65% to 2.56% as the defect density escalates from 10^{12} to 10^{18} cm^{-3}, as shown in Fig. 2. This phenomenon is distinct in the context of acceptor defects.

Similarly, in the case of the CdS Window layer, a distinct relationship between defect density and efficiency is established. Here, the efficiency exhibits a discernible decline from 16.56% to 13.82% as the defect density increases from 10^{12} to 10^{18} cm^{-3}, as shown in Fig. 3. This correlation underscores the influence of defect density on the performance of the solar cell in the context of both layers. The effect of different densities and defects charge types in the light-absorbing CdTe & CdS layer on the photovoltaic performance parameters of solar cell devices has been considered. It has been found that photovoltaic parameters retain their highest values of Voc, Jsc, FF, and η till a density of defects of 10^{12} cm^{-3}. This research indicates that there is an optimum defect density of 10^{12} cm^{-3}, above which the solar cell performance starts degrading.

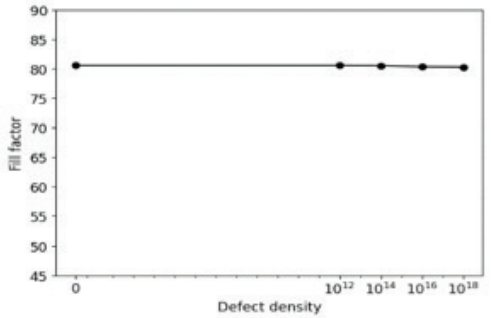

(a) Variation of Fill factor (FF) vs Defect density

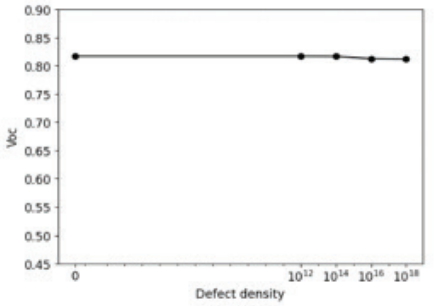

(b) Variation of open-circuit voltage (Voc) vs Defect density

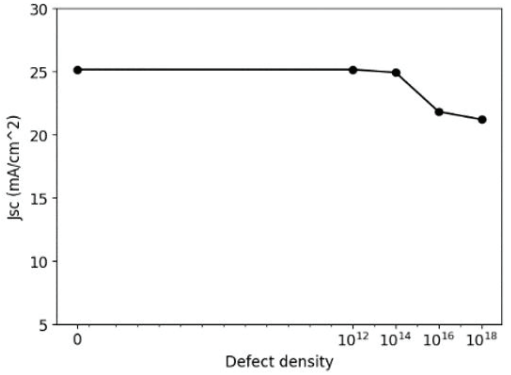

(c) Variation of Fill factor (FF) vs Defect density

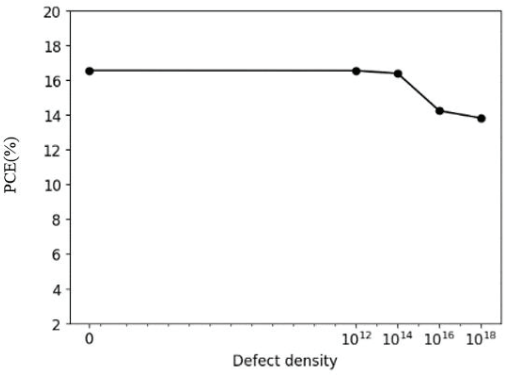

(d) Variation of percentage of the power Conversion Efficiency (PCE%) vs Defect density

Fig. 1. Effect of the donor defect density on FF, Jsc, Voc, and PCE (%) in the CdS window layer.

C. Spectral response

The concept of Quantum Efficiency (QE) revolves around the proportion of incident photons that are effectively captured by a solar cell's total charge carriers. In this investigation, we have generated four distinct QE curves shown in Fig. 4, with curves (a) and (c) delineating acceptor defects, while curves (b) and (d) portraying donor defects. These curves vividly illustrate the defect characteristics inherent to both the absorber and window layers. Examining the QE curve attributed to acceptor defects within the CdTe layer, a noticeable trend emerges wherein efficiency experiences a rapid decline in tandem with escalating defect density. This phenomenon is eloquently portrayed in Fig. 4. (a), which showcases the generated curves labeled 1(black), 2(red), 3(blue), and 4(green). Notably, curves 1 and 2, corresponding to defect densities of 10^{12} and 10^{14} cm^{-3}, exhibit a relatively similar efficiency drop. In contrast, curves 3 and 4, corresponding to defect densities of 10^{16} and 10^{18} cm^{-3}, demonstrate a substantial reduction in efficiency. An intriguing nuance surfaces beyond a wavelength of 500, where curve 4 notably flattens. This is attributed to heightened recombination and a concomitant decline in carrier collection, culminating in a noticeable reduction in quantum efficiency. In essence, these QE curves proficiently unveil the intricate interplay between defect density, carrier behavior, and quantum efficiency, shedding light on the dynamic response of the CdTe layer to varying fault densities.

The QE curve corresponding to donor defects is portrayed in Fig. 4. (b). this graph delineates a decline in efficiency as defects escalate, albeit at a slower pace compared to the absorber layer. This specific depiction pertains to the CdS layer's QE curve. Notably, the produced curves labeled 1, 2, 3, and 4 correspond to defect densities of 10^{12}, 10^{14}, 10^{16}, and 10^{18} cm^{-3}, respectively. It is intriguing to note that, akin to the acceptor defect case, curves 1 and 2 bear a similarity due to a relatively marginal efficiency drop between defect densities 10^{12} and 10^{14} cm^{-3}. However, noteworthy distinctions emerge when comparing curves 3 and 4 to curves 1 and 2. Notably, the size of donor defects being relatively small, the efficiency decrement is less pronounced as defect density increases. Moreover, the influence of recombination initially

intensifies for curves 3 and 4, followed by a subsequent decline in the later wavelengths. Consequently, curves 3 and 4 exhibit a characteristic dip and recovery in efficiency.

The delineation of the device's external quantum efficiency (QE) effectively captures the solar cell's functional wavelength range, thereby enhancing our insight into the operational dynamics of the investigated solar cell. This figure of merit is defined as the ratio between the effective photocurrent calculated through the cell and the source photocurrent which is in the form of [48] as in (1),

$$I_{src} = \frac{1}{hc} q\lambda P_b W_b \quad (1)$$

where λ is the photon wavelength, q is the electronic charge, c is the speed of light, h is Planck's constant P_b is the power density of the incident light, and W_b is the beam width clipped to the device [49].

As dictated by a given light source, the available photocurrent across the cell is intrinsically contingent upon the distinct optical attributes of the various materials at play. Mainly, we have adopted the wavelength-dependent refractive index (n) and extinction coefficient (k) of both CdS and CdTe layers, as elucidated by experimental extraction within the 250−1500 nm wavelength spectrum, as detailed in. Similarly, the optical characterization of the SnO_2 region was drawn.

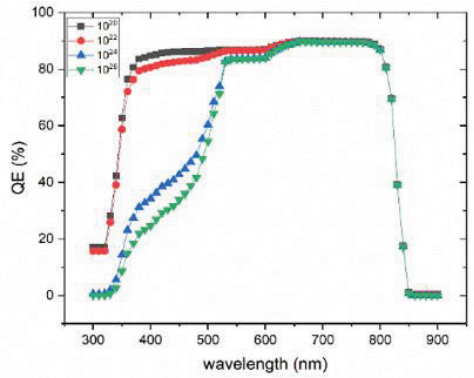

a) Variation of QE (%) vs wavelength for acceptor defect in CdTe Layer.

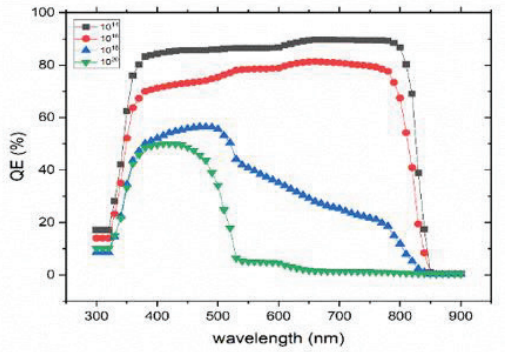

(b) Variation of QE (%) vs wavelength for Donor defect in CdS Layer.

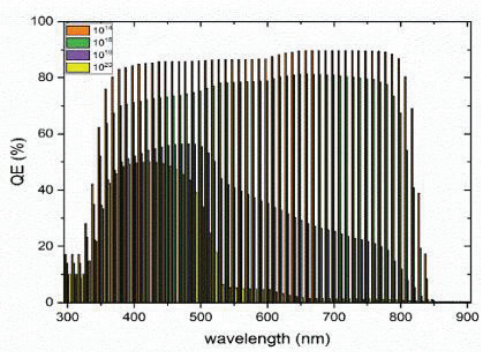

(c) Variation of QE (%) vs wavelength for acceptor defect in CdTe Layer by Bar curve

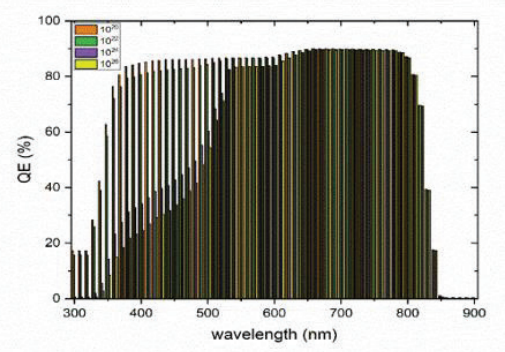

(d) Variation of QE (%) vs wavelength for Donor defect in CdS Layer By Bar curve

Fig. 2. Dependency of QE on defect density.

In Fig. 4, the external quantum efficiency (QE) profiles of both the reference and optimized cells are shown in detail. The QE behavior is demonstrated across a wavelength range from 300 nm to 950 nm. It is notable that the optimized configuration shows a clear increase in QE across the entire explored wavelength spectrum. This trend continues until the CdTe optical bandgap causes an absorption edge, which occurs around 850 nm. Particularly noteworthy is the peak of absorption within the range of $500 < \lambda < 800$ nm, where the average QE increases to approximately 96%, reaching a peak of 96.98% precisely at $\lambda = 650$ nm. The distinct absorption point at $\lambda = 500$ nm is a result of the inherent properties of the CdS material. It is also worth noting that for wavelengths below this critical value, light is primarily absorbed by the FTO layer. This comprehensive illustration of the QE behavior and its interaction with the optimized cell design is now complete.

IV. Conclusion

This study offers a thorough analysis of how defects impact the performance of CdTe solar cells. The focus is on acceptor and donor defects in the CdTe absorber and CdS window layers, respectively. Using the SCAPS platform, we calculated key parameters like efficiency, open-circuit voltage (Voc), short-circuit current density (Jsc), and fill factor (FF) across a range of defect densities from 10^{12} to 10^{18} cm^{-3}. Our findings show that acceptor defects are more prevalent in the CdTe layer, while donor defects primarily affect the CdS layer. Our simulations demonstrate that defect densities below 10^{12} cm^{-3} have minimal impact on the efficiency of both layers. However, as defect density increases beyond this threshold, all parameters, including Voc, Jsc, FF, and overall efficiency, exhibit a significant decline. The CdTe layer is more affected, where efficiency drops from 17.65% to 2.56% as acceptor defect density increases from 10^{12} to 10^{18} cm^{-3}. In contrast, donor defects in the CdS layer result in a smaller efficiency reduction, from 16.56% to 13.82%. The introduction of acceptor defects in the CdTe layer leads to the formation of trap levels, which evolve with increasing defect density. These traps, initially below the Fermi level, eventually lie between the Fermi level and the conduction band at higher densities, causing photo-generated electrons to become trapped and reducing photovoltaic efficiency. The absorber layer's characteristics are crucial, as efficiency is closely tied to its quality; hence, defects in this layer have a more pronounced impact. Spectral response analysis through Quantum Efficiency (QE) curves further elucidates the effects of defect density. The QE for acceptor defects in the CdTe layer shows a rapid efficiency decline with increasing defect density, especially beyond a wavelength of 500 nm, due to increased recombination and reduced carrier collection. For donor defects in the CdS layer, the decline is slower and less pronounced, with a characteristic dip and recovery in efficiency. This study highlights the critical role of minimizing defect densities in CdTe solar cells to optimize their performance. It emphasizes the need for improved materials and manufacturing processes to mitigate defects, particularly in the CdTe absorber layer, to enhance the efficiency and reliability of solar cell devices. Overall, this work contributes to a deeper understanding of the interplay between defect density and solar cell performance, providing valuable insights for future research and development in photovoltaic technology.

Acknowledgements

The authors gratefully acknowledge to the department of EEE, BSMRSTU to facilities the laboratory.

Conflict of Interest

The authors declare no conflict of interest in the publication process of the research article.

Author Contributions

Author 1: Data collection, analysis, writing – original draft preparation; Author 2: Supervision, draft review and editing, investigation; Author 3: Conceptualization, review; Author 4: Project administration; Author 5: Analysis, writing – original draft preparation.

References

[1] A. C. Lazaroiu, M. Gmal Osman and C.-V. Strejoiu, "A comprehensive overview of photovoltaic technologies and their efficiency for climate neutrality," *Sustainability,* vol. 15, no. 23, p. 16297, 2023.

[2] Ç. Çetinkaya, E. Çokduygulular and F. Güzelçimen, "Highly improved light harvesting and photovoltaic performance in CdTe solar cell with functional designed 1D-photonic crystal via light management engineering," *Scientific Reports,* vol. 12, no. 1, p. 11245, 2022.

[3] A. A. Pérez-Orozco, D. A. Liña-Martínez and M. Courel, "Towards a CdTe Solar Cell Efficiency Promotion: The Role of ZnO: Al and CuSCN Nanolayers," *Nanomaterials,* vol. 13, no. 8, p. 1335, 2023.

[4] M. A. Scarpulla, B. McCandless, A. B. Phillips, Y. Yan, M. J. Heben, C. Wolden, G. Xiong, W. K. Metzger, D. Mao, D. Krasikov, I. Sankin, S. Grover, A. Munshi, W. Sampath, J. R. Sites, A. Bothwell, D. Albin, M. O. Reese, A. Romeo, M. Nardone, R. Klie, J. M. Walls, T. Fiducia, A. Abbas and S. M. Hayes, "CdTe-based thin film photovoltaics: Recent advances, current challenges and future prospects," *Solar Energy Materials and Solar Cells,* vol. 255, p. 112289, 6 2023.

[5] I. Dharmadasa and A. Alam, "How to Achieve Efficiencies beyond 22.1% for CdTe-Based Thin-Film Solar Cells," *Energies,* vol. 15, no. 24, p. 9510, 12 2022.

[6] M. M. Uddin, C. Wang, C. Zhang and J. Ji, "Investigating the energy-saving performance of a CdTe-based semi-transparent photovoltaic combined hybrid vacuum glazing window system," *Energy,* vol. 253, p. 124019, 8 2022.

[7] H. Dang, E. Ososanaya and N. Zhang, "Improving reliability of window-absorber solar cells through CdS nanowires," *Optical Materials,* vol. 132, p. 112721, 10 2022.

[8] N. A. Aziz, C. K. Sheng and H. J. Jie, "Water remediation capability of cubic-phase CdS nanoparticles as photocatalyst on photodegradation of aqueous rhodamine 6G dye under UV irradiation," *Digest Journal of Nanomaterials and Biostructures,* vol. 18, no. 1, pp. 203-210, 3 2023.

[9] A. Çiriş, B. M. Başol, Y. Atasoy, A. Karaca, M. Tomakin, T. Küçükömeroğlu and E. Bacaksız, "Effect of ultra-thin CdSexTe1−x interface layer on parameters of CdTe solar cells," *Solar Energy,* vol. 234, pp. 128-136, 3 2022.

[10] B. Good, E. Colegrove and M. O. Reese, "Effects of absorber near-interface compensation on Cd(Se,Te) solar cell performance," *Solar Energy Materials and Solar Cells,* vol. 246, p. 111928, 102022.

[11] Y. Wang, G. Wang, Y. Zhou, Q. Xie, J. Chen, K. Zheng, L. Zheng, J. Pan and R. Wang, "Research progress in doped absorber layer of CdTe solar cells," *Renewable and Sustainable Energy Reviews,* vol. 183, p. 113427, 2023.

[12] P. Khaledi and M. Behboodnia, "Design and Simulation of a Cooling System for FTO/I-SnO 2/CdS/CdTe/Cu 2 O Solar Cells," *International Journal of Photoenergy,* vol. 2023, 2023.

[13] X. Mao, M. Bian, C. Wang, R. Zhou, L. Wan, Z. Zhang, J. Zhu, W. Chen, C. Shi and B. Xu, "Ultrathin SnO2 buffer layer aids in interface and band engineering for Sb2 (S, Se) 3 solar cells with over 8% efficiency," *ACS Applied Energy Materials,* vol. 5, no. 3, pp. 3022-3033, 2022.

[14] A. F. Palmstrom and M. O. Reese, "Ultrathin oxides for solar cells," *Ultrathin Oxide Layers for Solar and Electrocatalytic Systems,* pp. 27-69, 2022.

[15] A. Sharan, M. Nardone, D. Krasikov, N. Singh and S. Lany, "Atomically thin interlayer phase from first principles enables defect-free incommensurate SnO2/CdTe interface," *Applied Physics Reviews,* vol. 9, no. 4, 2022.

[16] H. Zhang, F. Qu and H. Li, "Front Transparent Passivation of CIGS-Based Solar Cells via AZO," *Molecules,* vol. 27, no. 19, p. 6285, 2022.

[17] A. Rayhan, M. Khan and M. R. Islam, "Enhancing CsSn0.5Ge0.5I3<Perovskite Solar Cell Performance via Cu2O Hole Transport Layer Integration," *International Journal of Photoenergy,* vol. 2024, no. 1, p. 1-17, 2024.

[18] C. Doroody, K. S. Rahman, P. Chelvanathan, M. A. Ibrahim, K. Sopian, N. Amin, S. Chowdhury and S. Channumsin, "Incorporation of Magnesium-doped Zinc Oxide (MZO) HRT Layer in Cadmium Telluride (CdTe) Solar Cells," *Results in Physics,* vol. 47, p. 1-6, 2023.

[19] C. Doroody, K. S. Rahman, T. S. Kiong and N. Amin, "Optoelectrical impact of alternative window layer composition in CdTe thin film solar cells performance," *Solar energy,* vol. 233, pp. 523-530, 2022.

[20] A. J. Clayton, A. Abbas, P. J. Siderfin, S. Jones, A. Teloeken, O. Oklobia, J. M. Walls and S. J. C. Irvine, "MOCVD of II-VI HRT/Emitters for Voc Improvements to CdTe Solar Cells," *Coatings,* vol. 12, no. 2, p. 261, 2022.

[21] T. P. Shalvey, H. Bagshaw and J. D. Major, "Interrelation of the CdTe Grain Size, Postgrowth Processing, and Window Layer Selection on Solar Cell Performance," *ACS applied materials & interfaces,* vol. 14, no. 37, pp. 42188-42207, 2022.

[22] A. Blakers, "Development of the PERC solar cell," IEEE Journal of Photovoltaics, vol. 9, no. 3, pp. 629-635, 2019.

[23] N. Chuchvaga, K. Zholdybayev, K. Aimaganbetov, S. Zhantuarov and A. Serikkanov, "Development of Hetero-Junction Silicon Solar Cells with Intrinsic Thin Layer: A Review," Coatings, vol. 13, no. 4, p. 796, 2023.

[24] R. Peibst, F. Haase, B. Min, C. Hollemann, T. Brendemühl, K. Bothe and R. Brendel, "On the chances and challenges of combining electron-collecting nPOLO and hole-collecting Al-p+ contacts in highly efficient p-type c-Si solar cells," Progress in Photovoltaics: Research and Applications, vol. 31, no. 4, pp. 327-340, 2023.

[25] S. Tepner and A. Lorenz, "Printing technologies for silicon solar cell metallization: A comprehensive review," Progress in Photovoltaics: Research and Applications, vol. 31, no. 6, pp. 557-590, 2023.

[26] I. E. Tinedert, A. Saadoune, I. Bouchama and M. A. Saeed, "Numerical modelling and optimization of CdS/CdTe solar cell with incorporation of Cu2O HT-EBL layer," Optical Materials, vol. 106, p. 109970, 2020.

[27] A. Agarwal, N. K. Singh and T. Kanumuri, "Device modelling of cdte photovoltaic cell using V2O5/Cu2O/NiO as a back surface field layer through numerical simulation," MAPAN, vol. 37, no. 2, pp. 387-398, 2022.

[28] C. A. Benisha and S. Routray, "Performance enhancement of kesterite solar cell with doped-silicon back surface field layer," Silicon, vol. 14, no. 13, pp. 8045-8054, 2022.

[29] M. H. Ali, M. A. Al Mamun, M. D. Haque, M. F. Rahman, M. K. Hossain and A. Z. Md. Touhidul Islam, "Performance Enhancement of an MoS2-Based Heterojunction Solar Cell with an In2Te3 Back Surface Field: A Numerical Simulation Approach," ACS omega, vol. 8, no. 7, pp. 7017-7029, 2023.

[30] M. N. Harif, C. Doroody, A. Nadzri, H. Nisham Rosly, N. I. Ahmad, M. Isah and N. Amin, "Effect of Cu2Te Back Surface Interfacial Layer on Cadmium Telluride Thin Film Solar Cell Performance from Numerical Analysis," Crystals, vol. 13, no. 5, p. 848, 2023.

[31] Z. Benbouzid, W. Benstaali, W. L. Rahal, N. Hassini, M. R. Benzidane and A. Boukortt, "Efficiency Enhancement by BSF Optimization on Cu (In1− x, Gax) Se2 Solar Cells with Tin (IV) Sulfide Buffer Layer," Journal of Electronic Materials, vol. 52, no. 7, pp. 4575-4586, 2023.

[32] G. Hashmi, M. S. Hossain and M. H. Imtiaz, "Electrical and optical parameter-based numerical simulation of high-performance CdTe, CIGS, and CZTS solar cells," Journal of Theoretical and Applied Physics, vol. 17, no. 3, 2023.

[33] Z. Hussain, M. M. Alharthi and S. S. M. Ghoneim, "Enhanced performance of thin-film amorphous silicon (a-Si) solar cells encapsulated with distributed Bragg reflector pairs," Journal of Computational Electronics, vol. 21, no. 4, pp. 852-858, 2022.

[34] C. F. Kamdem, A. T. Ngoupo, F. X. A. Abega, A. M. N. Abena and J.-M. B. Ndjaka, "Design and Performance Enhancement of a GaAs-Based Homojunction Solar Cell Using Ga 0.5 In 0.5 P as a Back Surface Field (BSF): A Simulation Approach," International Journal of Photoenergy, vol. 2023, 2023.

[35] E. Amoupour, S. G. Sarvelat, J. Hasanzadeh and A. A. Ziabari, "Simulation and improvement of the performance of CdTe solar cell with ultrathin absorber layer," Surface Review and Letters, vol. 29, no. 02, p. 2250021, 2022.

[36] G. P. Darshan, D. R. Lavanya, B. D. Prasad, S. C. Sharma and H. Nagabhushana, "Quantum dots-based solar cells: Futuristic green technology to accomplish the energy crisis," Quantum Dots, pp. 157-188, 2023.

[37] L. Wang, J. Wu, S. Wang, H. Liu, Y. Wang and D. Wang, "The reformation of catalyst: from a trial-and-error synthesis to rational design," Nano Research, 2023.

[38] D. Errandonea, F. Rodriguez, R. Vilaplana, D. Vie, S. Garg, B. Nayak, N. Garg, J. Singh, V. Kanchana and G. Vaitheeswaran, "Band-Gap Energy and Electronic d–d Transitions of NiWO4 Studied under High-Pressure Conditions," The Journal of Physical Chemistry C, 2023.

[39] G. Hashmi, M. S. Hossain and M. H. Imtiaz, "Electrical and optical parameter-based numerical simulation of high-performance CdTe, CIGS, and CZTS solar cells," Journal of Theoretical and Applied Physics, vol. 17, no. 3, 2023.

[40] P. Okoye, S. Azi and T. Qahtan, "Synthesis, properties, and applications of doped and undoped CuO and Cu2O nanomaterials," Materials Today Chemistry, vol. 30, no. 2468-5194, p. 101513, 2023.

[41] M. Barbato, E. Artegiani, M. Bertoncello and M. Meneghini, "CdTe solar cells: technology, operation and reliability," Journal of Physics D: Applied Physics, vol. 54, no. 0022-3727, p. 333002, 2021.

[42] L. Thomas, "N-Type Cdte Solar Cells: Doping and Devices," The University of Liverpool (United Kingdom), no. 9798380728294, 2023.

[43] K. H. Abass, A. Adil, A. J. Alrubaie, B. H. Rabee, A. M. Kadim, S. H. Talib, K. A. Mohammed and A. S. Jassim, "Fabrication and Characterization of p-SnS/n-Si Solar Cell by Thermal Evaporation Technique and the Effect of Ag-doped on Its Efficiency," International Journal of Nanoscience, vol. 22, no. 01, p. 2350003, 2023.

[44] A. Z. Arsad, A. W. M. Zuhdi, S. F. Abdullah, C. F. Chau, A. Ghazali, I. Ahmad and W. S. W. Abdullah, "Effect of Chemical Bath Deposition Variables on the Properties of Zinc Sulfide Thin Films: A Review," Molecules, vol. 28, no. 6, p. 2780, 2023.

[45] A. Bosio, "CdTe-Based Photodetectors and Solar Cells," Handbook of II-VI Semiconductor-Based Sensors and Radiation Detectors: Volume 2, Photodetectors, pp. 205-230, 2023.

[46] E. I. Emon, A. M. Islam, M. K. Sobayel, S. Islam, M. Akhtaruzzaman, N. Amin, A. Ahmed and M. J. Rashid, "A comprehensive photovoltaic study on tungsten disulfide (WS2) buffer layer based CdTe solar cell," Heliyon, vol. 9, no. 3, 2023.

[47] B. Z. Bhari, K. S. Rahman and P. Chelvanathan, "Numerical simulation of ultrathin CdTe solar cell by SCAPS-1D," IOP Conference Series: Materials Science and Engineering, vol. 1278, no. 1, p. 012002, 2023.

[48] G. Liang, Z. Li, M. Ishaq, Z. Zheng, Z. Su, H. Ma, X. Zhang, P. Fan and S. Chen, "Charge Separation Enhancement Enables Record Photocurrent Density in Cu2ZnSn (S, Se) 4 Photocathodes for Efficient Solar Hydrogen Production," Advanced Energy Materials, vol. 13, no. 19, p. 2300215, 2023.

[49] F. Xu, K. Gong, D. Liu, L. Wang, W. Li and X. Zhou, "Enhancing photocurrent of dye-sensitized solar cells through solvent modulating aggregation of dyes," Solar Energy, vol. 240, pp. 157-167, 2022.

[50] E. Artegiani, A. Gasparotto, M. Meneghini, G. Meneghesso and A. Romeo, "How the selenium distribution in CdTe affects the carrier properties of CdSeTe/CdTe solar cells," Solar Energy, vol. 260, pp. 11-16, 2023.

[51] A. Kumar, S. Mukherjee, H. Sharma, D. K. Rana, A. Kumar, R. Kumar and R. K. Choubey, "Fabrication of low-cost and fast-response visible photodetector based on ZnS: Mn/p-Si heterojunction," Materials Science in Semiconductor Processing, vol. 155, p. 107226, 2023.

[52] R. Kumar and A. Kumar, "Development of an efficient double absorber CIGSSe/perovskite solar cell with the combination of experimental data of Mg-doped CeO2 buffer layer," Optical Materials, vol. 139, p. 113731, 2023.

[53] A. R. Carrasco-Hernández, R. I. Ruvalcaba-Ontiveros, E. Martínez-Guerra, J. A. Duarte-Moller and H. E. Esparza-Ponce, "Evolution of Structural and Optical Properties of Cuprous Oxide Particles for Visible Light Absorption," Journal of Nanomaterials, vol. 2022, 2022.

[54] L. Marasamy, R. Aruna-Devi, O. I. D. Robledo, J. Á. C. Carvayar, N. E. V. Barragán, J. Santos-Cruz, S. A. Mayén-Hernández, G. Contreras-Puente, M. de la Luz Olvera and F. de Moure Flores, "Probing the significance of RF magnetron sputtering conditions on the physical properties of CdS thin films for ultra-thin CdTe photovoltaic applications," Applied Surface Science, vol. 574, p. 151640, 2022.

[55] V. Lahariya, M. Michalska-Domańska and S. J. Dhoble, "Synthesis, structural properties, and applications of cadmium sulfide quantum dots," Quantum Dots, pp. 235-266, 2023.

[56] J.-M. Wu, Y.-P. Lv, J.-Z. Wang, L. Yang, F. Wang, H. Wu and X.-H. Xu, "Performance improvement of Sb2Se3 thin-film solar cells through ultraviolet ozone treatment," Rare Metals, vol. 41, no. 8, pp. 2671-2679, 2022.